A Simple Model for Ion Flux-Energy Distribution Functions in Capacitively Coupled Radio-Frequency Plasmas Driven by Arbitrary Voltage Waveforms

Edmund Schüngel,* Zoltán Donkó, Julian Schulze

The ion flux-energy distribution function (IFEDF) is of crucial importance for surface processing applications of capacitively coupled radio-frequency (CCRF) plasmas. Here, we propose a model that allows for the determination of the IFEDF in such plasmas for various gases and pressures in both symmetric and asymmetric configurations. A simplified ion density profile and a quadratic charge voltage relation for the plasma sheaths are assumed in the model, of which the performance is evaluated for single- as well as multi-frequency voltage waveforms. The IFEDFs predicted by this model are compared to those obtained from PIC/MCC simulations and retarding field energy analyzer measurements. Furthermore, the development of the IFEDF shape and the ion dynamics in the plasma sheath region are discussed in detail based on the spatially and temporally resolved model data.

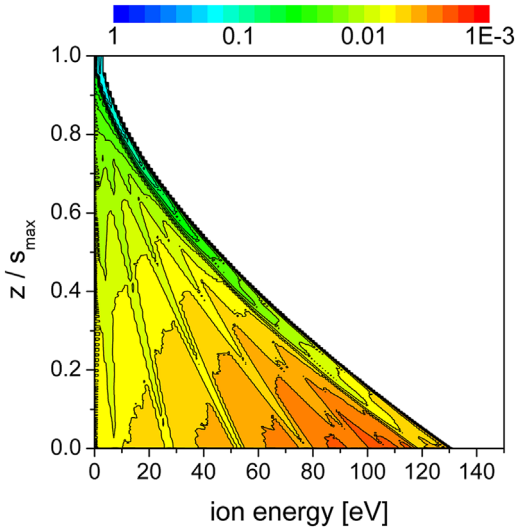

1. Introduction

When it comes to modern surface modification processes such as the highly selective and strongly anisotropic etching of nanometer sized structures in the semiconductor manufacturing industry, capacitively coupled radio frequency (CCRF) plasmas are typically the tools of choice.[1,2] These plasmas provide unique opportunities to adjust the fluxes and impact energies of reactive and ionic species, which are most important for the processes at the surface. The typical discharge configurations are either geometrically asymmetric (a relatively small powered electrode in a large vacuum chamber) or geometrically symmetric (two large electrodes in a plane-parallel setup), depending on the

Dr. E. Schüngel, Dr. J. Schulze
Department of Physics, West Virginia University, Morgantown, West Virginia 26506-6315, USA
E-mail: edmundSchuengel@gmx.net
Dr. E. Schüngel
Evatec AG, Hauptstrasse 1a, Trübbach CH-9477, Switzerland
Dr. Z. Donkó
Wigner Research Centre for Physics, Institute for Solid State Physics and Optics, Hungarian Academy of Sciences, Konkoly-Thege Miklós str. 29-33, Budapest 1121, Hungary
Dr. J. Schulze
Institute for Electrical Engineering, Ruhr-University Bochum, Bochum 44780, Germany

specific application.[3] In the symmetric single-frequency situation, the particle fluxes and energies are equal at both electrodes, whereas they differ from each other in an asymmetric situation. This occurs because the voltage drop across the sheaths adjacent to the surfaces is affected by the geometry, hence causing different energy gains of ions adjacent to either electrode. Furthermore, the different voltage drops across the two sheaths also lead to different electron power absorption rates in the two sheath regions, hence causing an asymmetric ionization rate. As a consequence, the plasma density profile and the ion flux become asymmetric with respect to the discharge center.

Several methods of adjusting the ion energy, or more specifically the ion flux-energy distribution function (IFEDF), have been developed to control and improve the ion bombardment in CCRF plasmas. Besides the physical setup of the electrodes and the vacuum chamber, the gas pressure and the driving voltage are the two main control quantities. It has been shown, however, that in single-frequency CCRF plasmas it is not possible to control the ion energy without affecting the ion flux.[4] Since such an independent control is highly desired, multi-frequency CCRF plasmas are widely used. One way to achieve separate control is the application of a driving voltage consisting of a low frequency component and a high frequency component. If the frequencies differ by about one order of magnitude, separate control of ion energy and ion flux is possible[5–8] within the limitations of the disturbing influences of the frequency coupling and of secondary electrons.[9,10] Another way to achieve separate control is the application of a voltage waveform consisting of a fundamental frequency and its subsequent harmonics.[11–31] Here, the phase angles between the applied harmonics serve as control parameters of the voltage waveform. For instance, waveforms with different absolute values of the global maximum and minimum[11–25,29–31] or different rising and falling slopes[26–28] can be generated, providing a method to control the symmetry of the discharge, the sheath dynamics and the ion energy at the two electrodes.

Using such advanced methods of customized driving voltage waveforms, the mean ion energy[11–31] as well as the shape of the IFEDF[18,30,32,33] can be controlled. Thus, the ion impact on a surface in a CCRF plasma can be tailored for specific applications.[21–24] However, the dynamics of the sheath electric field, as well as the ion kinetics in the sheath become more complicated. In single-frequency CCRF plasmas, the IFEDF has been studied for decades (see, ref.[34] and references therein). Several studies focused on the bimodal shape in the IFEDF caused by ions, that cross the sheath without collisions.[8,31,34,35] Furthermore, the role of collisional redistribution of ions within the IFEDF,[34,36–41] of the total sheath voltage,[42] as well as of the ion dynamics at reduced driving frequencies[35,39,42–44] have been investigated. Various approaches of modeling the IFEDF in single-frequency CCRF plasmas can be found in the literature.[36,38–40,45] Wild and Koidl developed a model for the IFEDF in such single-frequency CCRF plasmas and studied, how the different ion flux components of the IFEDF are formed.[36] Recently, a model allowing for a detailed analysis of the ion dynamics in a single-frequency CCRF plasmas has been discussed by Chen and Pu.[39] Up to now, a model for the IFEDF in multi-frequency CCRF plasmas driven by customized voltage waveforms is missing. The approach proposed by Coumou et al. provides a first insight into the formation of the IFEDF behind a multi-frequency RF sheath, but it is limited to the collisionless case.[30] A predictive control and an easy access to understand the features of the IFEDF in multi-frequency plasmas is highly desired to make such methods attractive for applications.

Here, we propose a model for the IFEDF and the ion dynamics in CCRF plasmas driven by multiple radio frequencies. It is based on the knowledge of the temporal evolution of the sheath voltage from a voltage balance model and an approximation of the spatial profiles of the ion density, as used by Wild and Koidl in their model of single-frequency discharges.[36] We compare the outcome of this model to the IFEDFs obtained from self-consistent particle-in-cell simulations with Monte Carlo treatment of collision processes (PIC/MCC), as well as with measured data. This comparison shows that the model allows for a simple but accurate determination of the IFEDF. The model is validated for symmetric, as well as asymmetric single- and multi-frequency discharges. We restrict ourselves to the investigation of the IFEDF only at the grounded electrode, although the model works equally well for the IFEDF at the powered electrode. In the single-frequency case, a voltage waveform of $\phi_\sim(t) = \phi_0 cos\,(2\pi f t)$ is applied, while in a triple-frequency discharge the voltage waveform is varied by tuning the phase angles,

$$\phi_\sim(t) = \sum_{i=1}^{3} \phi_i cos\,(i2\pi f + \theta_i), \tag{1}$$

where ϕ_i and θ_i are the individual harmonics' amplitudes and phases. We note that the model is not limited to such waveforms and can be used for arbitrary voltage waveforms as well as for CCRF plasmas driven by a low and a high frequency component. Further, it can be used to gain a detailed insight into the dynamics of the ions within the sheath. This is important for an understanding of the development of all features in the IFEDF, so that a further improvement of the IFEDF control is facilitated.

This paper is structured in the following way: The model is introduced in the next section. After explaining the basics and discussing the assumptions of the model, information

on the PIC/MCC method and the experimental setup is provided. Then, the results are presented and discussed in section 3, which is divided into three parts – the proof of concept of the model in single-frequency CCRF plasmas, in multi-frequency CCRF plasmas, and a detailed analysis of the ion dynamics in the model. Finally, conclusions are drawn in the last section.

2. Model, Simulation, and Experiment

2.1. IFEDF Model

The model considers the sheath region formed in a discharge consisting of a single, positively charged ion species, and electrons. The CCRF plasma can be generated by a voltage waveform of arbitrary shape, but the period of the lowest driving frequency must be shorter than the ion transit time through the sheath region. This is required to justify the assumption of a temporally constant ion density. The basic idea of the model is that the IFEDF at the electrode is composed of two components. "Primary" ions, that flow from the quasi-neutral plasma bulk zone into the sheath region, are accelerated by the electric field over the entire sheath region, and arrive at the electrode without collisions at relatively high energies. If the transit time of these primary ions is much longer than the RF period of the lowest applied frequency, they generate a rather narrow peak in the IFEDF at an energy corresponding to the mean sheath voltage. For shorter ion transit times of only a few RF periods, the peak spreads to lower and higher energies.[34] The other component of the IFEDF are "secondary" ions that are created in charge-exchange collisions of ions with the neutral background gas. In many situations, these collision processes are dominant. After the charge transfer, the former ion proceeds as a fast neutral and the former neutral gas particle becomes positively charged, starts with negligible (thermal) velocity, and is accelerated toward the electrode.

The simplified mathematical description of the ion density profile, $n_i(z)$, in the plasma sheath region, that has been used by Wild and Koidl for their model of IFEDFs in strongly asymmetric single-frequency CCRF plasmas,[36] is adopted here:

$$n_i(z) \approx n_0 \left[1 - \frac{z}{s_{g,max}}\right]^{-1/2}, \tag{2}$$

where $s_{g,max}$ is the maximum extension of the grounded electrode sheath (occuring at the time of maximum applied voltage and maximum grounded electrode sheath voltage). The z-axis is perpendicular to the electrode surface (situated at $z=0$) and is directed toward the center of the discharge, and n_0 is a constant density at the electrode surface. Certainly, Equation (2) is a strong simplification, and more sophisticated theories to describe the density and field profiles in the voltage driven RF sheath are available (see ref.[46–48] or the recent works of Czarnetzki,[49] as well as of Chabert and Turner,[50] for instance). However, we choose the simple formula above, because it is our intention to keep this model as simple as possible, while still achieving a good agreement of the resulting IFEDF with the outcome of self-consistent simulations and experiments, as will be shown below. For the same reason, the exponent in Equation (2) is fixed to $-1/2$ in this work, whereas a slight variation was allowed in the original work of Wild and Koidl.[36]

In order to determine the voltage drop across the sheaths and the sheath widths, it is convenient to express these quantities as a function of the net charge in the respective sheath. In the following, we describe the derivation of the voltage drop across and the width of the grounded electrode sheath, because the IEDFs at the grounded electrode will be discussed in the results section; the properties of the powered electrode sheath can be determined in a similar procedure. The underlying model has been used in several studies of multi-frequency plasmas before.[11–13,15–17,51] A central assumption is that the total net charge within the entire discharge volume, Q_{tot}, is purely located in the two sheaths, that is, $Q_{tot} = Q_{sp}(t) + Q_{sg}(t)$, and that it is constant in time.[16] The charges in the powered electrode sheath, $Q_{sp}(t)$, and in the grounded electrode sheath, $Q_{sg}(t)$, change as a function of time within the RF period. Further, the approximation of a quadratic charge voltage relation of the sheaths is used here. An analytical treatment would not be possible, if the cubic correction[52,53] was included. The time dependent normalized charge in the grounded electrode sheath is found as[13,51]

$$\begin{aligned} q_{sg}(t) &= q_{tot} - q_{sp}(t) \\ &= \frac{q_{tot} - \sqrt{\varepsilon q_{tot}^2 - (1-\varepsilon)\frac{\eta + \phi_\sim(t)}{\phi_{tot}}}}{1-\varepsilon}. \end{aligned} \tag{3}$$

Here, all charges are normalized by $Q_0 = A_p\sqrt{2e\varepsilon_0 \bar{n}_{sp}\phi_{tot}}$ with A_p being the surface area of the powered electrode and $\bar{n}_{sp}$ being the mean ion density in the powered electrode sheath region, that is, $q_{tot} = Q_{tot}/Q_0$, $q_{sp} = Q_{sp}/Q_0$, and $q_{sg} = Q_{sg}/Q_0$, η and $\phi_\sim(t)$ are the DC self-bias and the applied voltage, ϕ_{tot} is the applied voltage amplitude.[13,51] The symmetry of the discharge is taken into account in the model via the symmetry parameter[11,13]

$$\varepsilon = \left|\frac{\phi_{sg}^{max}}{\phi_{sp}^{max}}\right|, \tag{4}$$

that is, as the absolute value of the ratio of the maximum voltage drops across the grounded and powered electrode sheaths. Both the symmetry parameter and the total charge can easily be determined from the DC self-bias, η, and from

the global extrema of the applied voltage waveform,[12,51] $\phi_{\sim,\max}$ and $\phi_{\sim,\min}$, via $\varepsilon = -\left(\eta + \phi_{\sim,\max}\right)/\left(\eta + \phi_{\sim,\min}\right)$ and $q_{tot} = \sqrt{\left(\phi_{\sim,\max} - \phi_{\sim,\min}\right)/[\phi_{tot}\,(1+\varepsilon)]}$. The time dependent voltage drop across the grounded electrode sheath is then

$$\phi_{sg}(t) = \varepsilon\phi_{tot}\left[q_{sg}(t)\right]^2. \tag{5}$$

It should be noted that the time-dependent charge located in the grounded electrode sheath, $q_{sg}(t)$, in the model above reaches a minimum of zero.[16] Hence, the sheath fully collapses and the predicted minimum sheath voltage is $\phi_{sg} = 0$. However, in reality a residual (RF floating) potential remains at the time of collapsing sheath to prevent a too high electron flux to the electrode.[1,2] This floating potential can become important for the ion dynamics, especially in situations when the amplitude of the time varying sheath voltage is relatively low, that is, when using a low driving voltage amplitude and/or in strongly asymmetric situations. We incorporate the floating potential by adding a constant component to the overall sheath voltage

$$\phi^*_{sg}(t) = \phi_{sg}(t) + \phi_{sg,fl}. \tag{6}$$

The floating potential is determined from the constraint of equal fluxes of positive and negative charges to either electrode, because any DC current component is prohibited in the steady state of the CCRF discharge by the presence of a blocking capacitor in the matching network. Hence, we adopt the standard approach (discussed by Lieberman,[1] for instance) and find the floating potential from the required time-averaged balance

$$\frac{1}{T_{rf}}\int_0^{T_{rf}}\sqrt{\frac{k_B T_e}{m_i}}dt = \frac{1}{T_{rf}}\int_0^{T_{rf}}\sqrt{\frac{k_B T_e}{2\pi m_e}}\exp\left\{-\frac{e\phi^*_{sg}(t)}{k_B T_e}\right\}dt \tag{7}$$

of the ion flux (Γ_i, left hand side of Equation (7)) and the electron flux (Γ_e, right hand side of Equation (7)) to the grounded electrode. (Note that an analytic solution cannot be found for multi-frequency scenarios.) Here, the usual assumptions[1] of an ion velocity close to the Bohm velocity ($u_i \approx u_B = \sqrt{k_B T_e/m_i}$) when entering the sheath, of a Maxwellian electron energy distribution function (with temperature T_e), of a constant ion flux within the sheath, and of a static and quasi-neutral plasma outside of the sheath ($n_i = n_e$) are made.

The time dependent sheath width is obtained in the following way: Assuming that the electron density equals the ion density in the plasma bulk region and instantaneously drops to zero at the sheath edge (known as step model of the plasma sheath[1,2]), the value of $q_{sg}(t)$ normalized by its maximum at any time within the RF period corresponds to the normalized integral of the ion density profile between the electrode (at $z = 0$) and the momentary position of the plasma sheath edge at the grounded electrode, $s_g(t)$. This yields

$$\frac{q_{sg}(t)}{q_{sg,max}} = \frac{\int_0^{s_g(t)} n_i(z)dz}{\int_0^{s_{g,max}} n_i(z)dz} = 1 - \sqrt{1 - \frac{s_g(t)}{s_{g,max}}} \tag{8}$$

using Equation (2) for the ion density profile. Thus, applying the quadratic charge voltage relation of the sheath again, the sheath edge is found as

$$s_g(t) = s_{g,max}\left[1 - \left(1 - \sqrt{\frac{\phi_{sg}(t)}{\phi_{sg,max}}}\right)^2\right]. \tag{9}$$

Both primary and secondary ions are accelerated in the RF electric field, which is high in the oscillating sheath region and approximately zero in the quasi-neutral plasma bulk region, that is, any residual effects of the ambipolar electric field[54] on the IFEDF are neglected. The electric field profile is determined via Poisson's equation by integrating the ion density profile spatially: $E_{sg}(z,t) = (e/\varepsilon_0)\int_{s(t)}^{z} n_i(z')\,dz'$. This yields

$$E_{sg}(z,t) = -\frac{3}{2}\frac{\phi_{sg,max}}{s_{g,max}}\left[\sqrt{1 - \frac{z}{s_{g,max}}} - \sqrt{1 - \frac{s_g(t)}{s_{g,max}}}\right]. \tag{10}$$

Here, $\phi_{sg,max} = (4en_0)/(3\varepsilon_0)$, obtained from integrating Poisson's equation once more, has been introduced.

We analyze the ion dynamics in the sheath by following the trajectory of ions space and time resolved, similar to the approach of Shihab et al.[55] and Chen and Pu.[39] The starting positions of these ions, (z_0, t_0), are homogeneously distributed in space (between $z = 0$ and $z = s_{g,max}$) and time (between $t = 0$ and $t = T_{rf}$). All these ions are traced and do not undergo any collisions. All ions that start within the sheath are secondary ions. The IFEDF is obtained at the grounded electrode by collecting the ions arriving at the electrode in energy "bins." The result is the flux density of ions within the respective energy interval. The according distribution function is called ion flux-energy distribution function (IFEDF) here; it is also called ion energy distribution function or ion flux distribution function in the literature. If the arriving ion is a primary ion, the ion flux in the respective bin is increased by $\Gamma_0\exp\left\{-s_{g,max}/\Lambda_{cx}\right\}$; if it is a secondary ion, that is, an ion created in a charge exchange collision within the sheath region, the ion flux in the respective bin is increased by $\Gamma_0\exp\left\{-\left(s_{g,max} - z\right)/\Lambda_{cx}\right\}s_{g,max}/\Lambda_{cx}$.[39] The factors in the expressions for the fluxes are required to account for the probability of collisions. Γ_0 is the constant that determines the total ion flux of the IFEDF. Here, we intend to focus on the shape of the IFEDF and, therefore, set

Γ_0 so that $\int f(E_i)\,dE_i = 1$. The additional factors in the flux of primary and secondary ions account for the probability, that these ions arrive at the electrode without undergoing collisions.[39] Only charge-exchange collisions are considered in the ion mean free path, Λ_{cx}. Although, the respective cross section may depend on the ion energy, it does not change by more than 10% over a wide energy region in case of argon ions.[56] Thus, we use the value of Λ_{cx} according to the cross section for charge exchange (elastic backscattering) at 10 eV.

In summary, the model is based on approximations of the ion density profile in the sheath (Equation (2)) and of the temporal evolution of the sheath voltage from an equivalent circuit model (Equation (6)). Therefore, the approach proposed here allows the investigation of the ion dynamics in the rf sheath and the determination of the IFEDF in a wide range of gas pressures, voltage amplitudes, frequencies, waveform shapes, and geometric configurations. Certainly, this range is limited by the underlying physical assumptions: for instance, the assumption of charge-exchange collisions with an energy-independent cross section being the dominant ion-neutral interaction would fail for most molecular gases or for too low sheath voltages, where ions would move mostly at low energies and the treatment of collisions would be more complicated. Based on the input parameter (applied voltage, DC self-bias, maximum sheath width, floating potential, mean free path), the ion motion in the sheath and the IFEDF are calculated within a few minutes.

2.2. PIC/MCC Simulation

The results of the model are compared to those obtained from self-consistent simulations. In the particle-in-cell simulation with Monte Carlo treatment of collisions (PIC/MCC) code,[4] the motion of about 10^5 superparticles representing argon ions or electrons is traced between the two infinitely large, parallel plate electrodes. The cross section data set of Phelps[56–58] is implemented for the treatment of collisions. The neutral gas pressure is varied, while the neutral gas temperature is kept at 350 K. Ions are lost at the electrode surfaces and release secondary electrons with a probabilty of 0.1. A probability of 0.2 is assumed for the reflection of electrons flowing onto the electrode surfaces.[59]

Although, the 1d3v code represents a geometrically symmetric discharge configuration, a DC self-bias may develop, due to the application of a voltage waveform that induces an asymmetry. In such cases, the DC self-bias is adjusted in the simulation in an iterative manner,[4] so that the losses of positive charges (ions) and negative charges (electrons) are equal on time average at either electrode surface, as it is the case in usual experimental setups of CCRF plasmas in steady state due to the presence of a blocking capacitor.

2.3. Experiment

The experimental setup consists of a modified Gaseous Electronics Conference (GEC) reference cell, where a parallel plate configuration is realized between the bottom (powered) and top (grounded) electrodes. The electrodes are 10 cm in diameter and are separated by a distance of 4 cm. The plasma is confined in this gap radially by a glass cylinder, which effectively enhances the grounded surface area due to the capacitive coupling to the chamber wall. Therefore, a geometrical asymmetry is present in the experiment. Further details on the experimental setup and discharge configuration can be found in a recent paper.[51] The discharge is operated in argon at 5 Pa pressure. The driving voltage consists of three RF harmonics: 13.56, 27.12, and 40.68 MHz. These harmonics are phase locked, so that the individual amplitudes and relative phases are controlled, and are applied to the electrode via a matching network.[29] In the experiment, the IFEDF is measured using an Impedans Semion Retarding Field Energy Analyzer (RFEA).[8] The device is implemented into the grounded electrode.

3. Results

In this section, the IFEDFs obtained from the model, the simulations, and the experiments will be presented and discussed. In the IFEDF, as well as in all other discussions of the ion dynamics in the sheath, the ion energy refers to the kinetic energy of the ions corresponding to the axial velocity component. (It actually is an ion velocity component, v_z, distribution function, which is conveniently evaluated as a function of the respective kinetic energy $mv_z^2/2$).[35] All IFEDFs are shown normalized with respect to the total ion flux, that is, $\int_0^{E_{i,max}} f(E_i)\,dE_i = 1$.

3.1. IFEDFs in Single-Frequency CCRF Plasmas (Model and PIC)

Figures 1 and 2 show the IFEDFs at the grounded electrode of a symmetric single-frequency CCRF plasma obtained from PIC/MCC simulations and predicted by the model, at various gas pressures, driving frequencies, and driving voltage amplitudes. Very good agreement is found between the two sets of data. The model uses the sheath width calculated from the simulation data using the criterion according to Brinkmann[60] as input parameter. The floating potential has been included, too, but it has a negligible effect.

For the same voltage amplitude, a higher driving frequency leads to a more efficient electron power absorption, thereby enhancing the ionization rate and plasma density. Thus, the sheath width becomes smaller

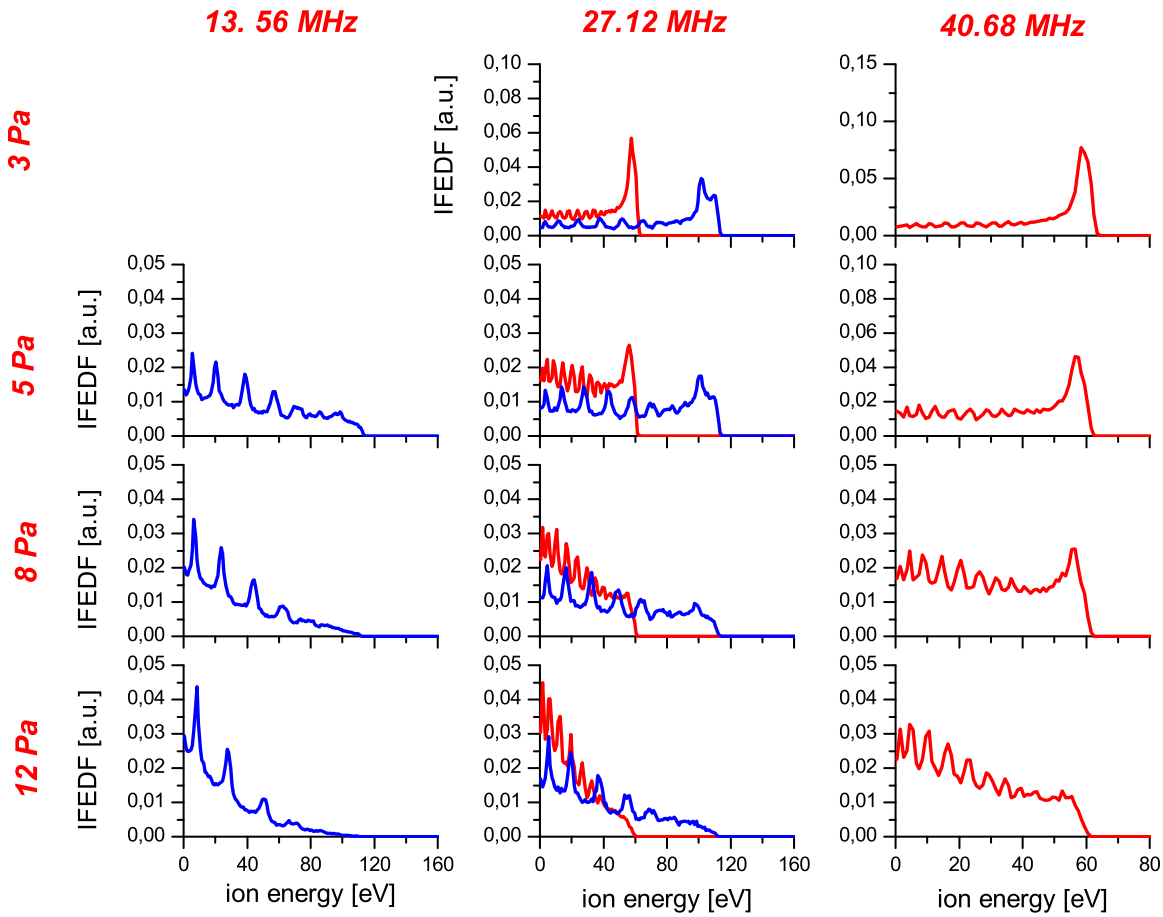

Figure 1. IFEDFs at the grounded electrode of a symmetric capacitive single-frequency discharge obtained from PIC/MCC simulations in argon for various pressures and base frequencies. The driving voltage amplitude is 120 V (red) or 240 V (blue).

and the probability of collisions of ions moving through the sheath region, becomes lower. Therefore, the fraction of high energy ions in the IFEDF is enhanced. Also, a reduction of the gas pressure leads to a less collisional motion of the ions through the sheath region and, hence, a higher mean ion energy. This is due to the fact that the mean free path is inversely proportional to the gas pressure. Although, the plasma density is smaller and the sheath width is larger at a reduced pressure, the ratio of the mean free path over the maximum sheath width becomes larger at lower pressures and, therefore, the collision probability becomes lower. Ions predominantly undergo charge-exchange collisions during their motion through the rf sheath. As a consequence, the IFEDF exhibits a broad spectrum with distinct peaks at low and intermediate energies. The effect of charge-exchange collisions on the ion dynamics is discussed based on the model results in the subsection IIIC. Furthermore, a change of the applied voltage amplitude at 27.12 MHz causes a change of the width of the IFEDF, as the maximum ion energy is proportional to the sheath voltage and, accordingly, to the applied voltage amplitude. However, the overall shape of the IFEDF does not change significantly. The effect of a larger sheath voltage and a higher plasma density at higher applied voltage amplitudes compensate each other, so that the sheath width and, therefore, the ion collision probability depends only very weakly on the voltage amplitude. Two different voltage amplitudes were chosen, because the simulation does not converge at the lowest frequency of 13.56 MHz for too low voltage amplitudes or at the highest frequency of 40.68 MHz for too high voltage amplitudes.

The general shapes of the IFEDFs as well as the trends as functions of pressure and frequency, respectively, agree well with experimental observations discussed in the literature (see refs.[8,34,35,41,61–63] for example).

3.2. IFEDFs in CCRF Plasmas Driven by Customized Voltage Waveforms (Model, PIC, and Experiment)

Figures 3(a) and (b) show the IFEDF at the grounded electrode of a geometrically symmetric, electrically asymmetric CCRF plasma obtained from the PIC/MCC simulation

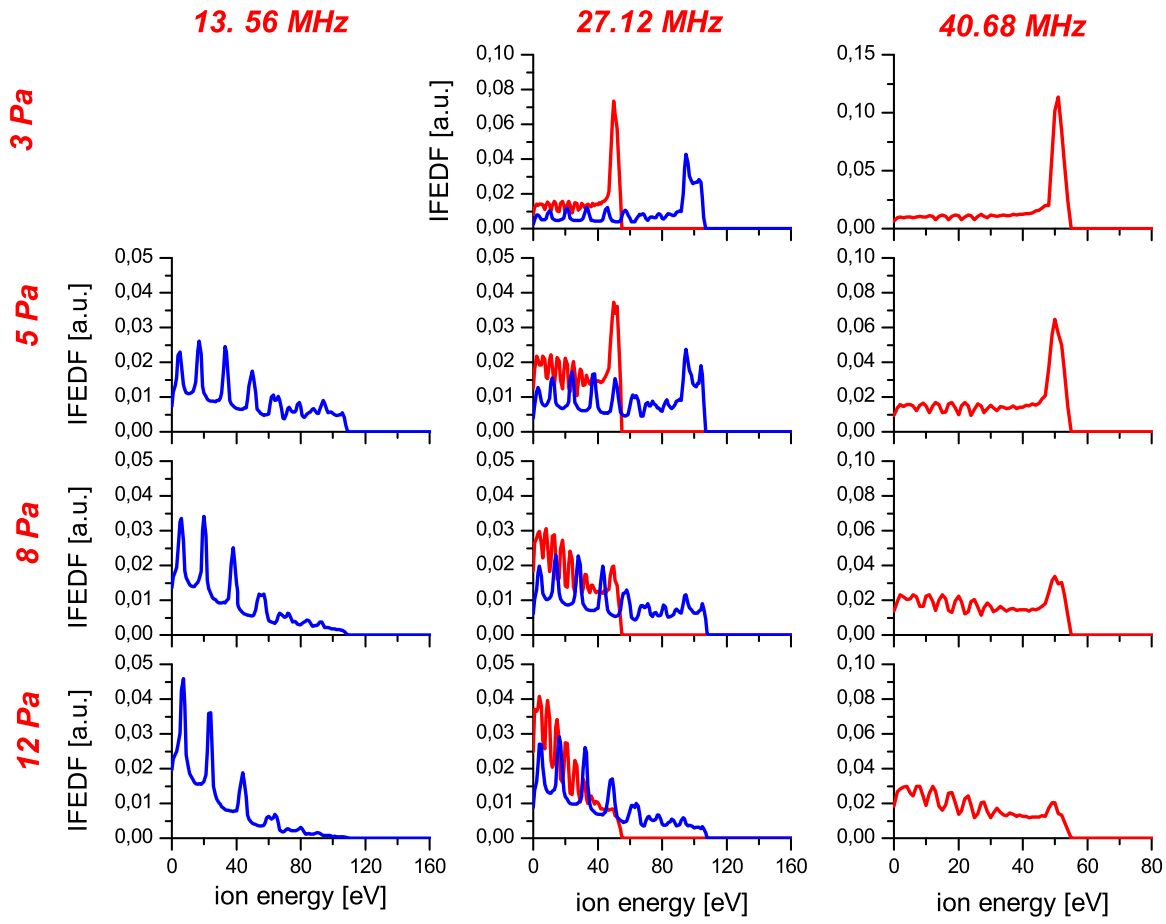

Figure 2. IFEDFs at the grounded electrode of a symmetric capacitive single-frequency discharge obtained from the model in argon for various pressures (mean free paths) and base frequencies. The driving voltage amplitude is 120 V (red) or 240 V (blue).

and based on the model. Here, a voltage waveform consisting of three consecutive harmonics is applied to the powered electrode. The phase angle of the 27.12 MHz component (θ_2, see Equation (1)) is varied, whereas the phase angle of the fundamental frequency at 13.56 MHz and of the 40.68 MHz component are kept zero. It has been shown before,[29,51] that the DC self-bias and the ion energy can effectively be controlled by tuning θ_2 only.

Overall, we find very good agreement between the results of the simulation and the model. All features of the IFEDFs determined in the PIC/MCC simulations are reproduced by the model. Again, the model uses the sheath width and the floating potential as the only simulation-based input parameter. Similarly, to the findings of previous studies,[29,51] the IFEDF shape and mean and maximum ion energy can be controlled by tuning the phase angle of the second harmonic. The $\theta_2 = 180^\circ$ case will be examined in great detail further below.

Figures 4(a) and (b) show the IFEDF at the grounded electrode of a geometrically and electrically asymmetric CCRF plasma obtained from RFEA measurements and the model. Again, a voltage waveform consisting of three consecutive harmonics is applied to the powered electrode, and the phase angle of the 27.12 MHz component is varied.

The experimentally determined IFEDFs exhibit a peak at the high energy end, as the mean free path of the ions is long enough at a gas pressure of 5 Pa to allow for a large fraction of the primary ions to arrive at the electrode without collisions. This peak in the IFEDF is found at considerably lower energies than that of the ions with highest energy in the simulation, that is, the maximum ion energy is lower in the measurements than in the simulation (see Figure 5(a)). This is due to the fact that the discharge is not geometrically symmetric. Therefore, the control range of the DC self-bias is shifted toward more negative values, although the control interval itself (difference between η at $\theta_2 = 0^\circ$ and at $\theta_2 = 180^\circ$) is hardly affected (see Figure 5(b)). Accordingly, the voltage drop across the grounded electrode sheath is reduced.

Moreover, the measured IFEDFs do not show any peaks at lower energies or other fine structures, as such details

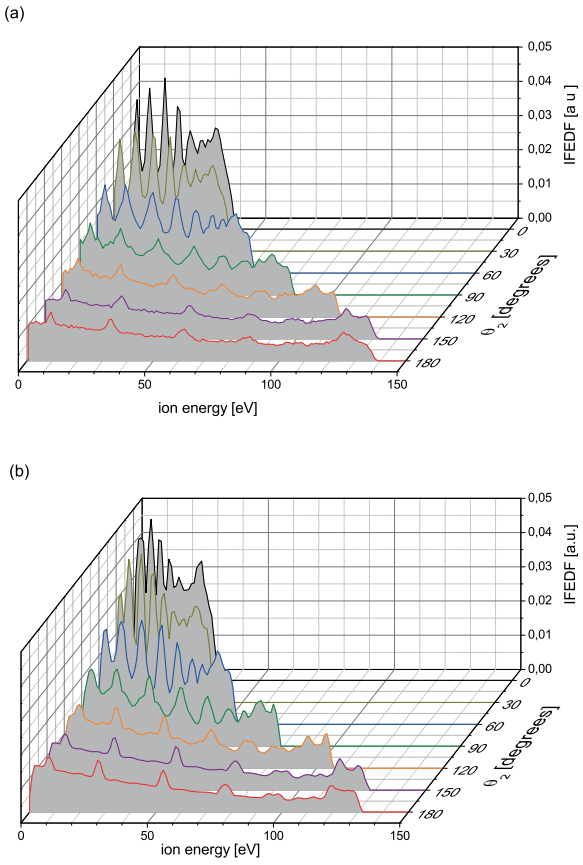

Figure 3. IFEDFs at the grounded electrode of an electrically asymmetric capacitive triple-frequency discharge obtained from (a) PIC/MCC simulations and (b) the model, in argon at 5 Pa for various phase angles of the second harmonic component. The voltage amplitudes are 120 V at 13.56 MHz + 80 V at 27.12 MHz + 40 V at 40.68 MHz. The phases θ_1 and θ_3 are set to 0°.

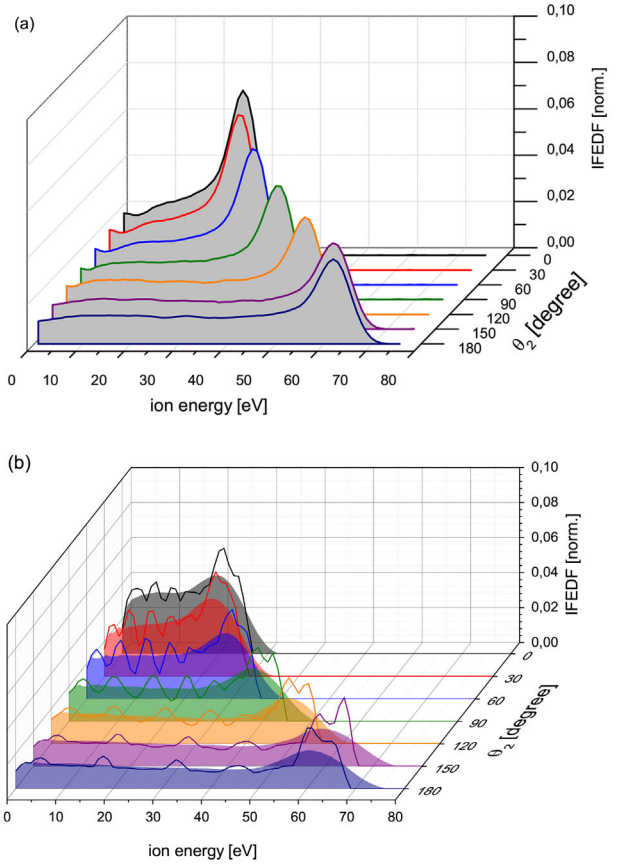

Figure 4. IFEDFs at the grounded electrode of a capacitive triple-frequency discharge obtained from (a) measurements by the RFEA in the geometrically asymmetric experimental setup and (b) the model, in argon at 5 Pa for various phase angles of the second harmonic component. The voltage amplitudes are 120 V at 13.56 MHz + 80 V at 27.12 MHz + 40 V at 40.68 MHz. The phases θ_1 and θ_3 are set to zero. The colored areas in (b) are obtained by averaging the model IFEDFs.

cannot be resolved by the RFEA, due to the limited energy resolution of the device, that we find to be of the order of about 10 eV. In order to compare the model with the experimental results, the imperfect energy resolution is emulated by applying an averaging over adjacent data points in the model. After that procedure, the overall shapes of the modeled IFEDFs (shaded areas in Figure 4(b)) resemble the measured ones. The sheath width is varied in the model until the ratio of mean ion energy over maximum ion energy matches the one determined from the measured IEDFs. A shorter sheath width leads to less collisions of ions in the sheath region and, therefore, a higher mean ion energy. Therefore, the mean ion energy typically is a monotonic function of the sheath width and the optimum agreement between measured and modeled IFEDF is found in a simple way. We find $s_{g,max} \approx 3$ mm for all phase angles.

3.3. Advanced Analysis of Example Case

In order to demonstrate how the model can be used to analyze the ion dynamics in the sheath region and the development of the IFEDF on a detailed level, the case of a geometrically symmetric triple-frequency CCRF plasma with phase angles $\theta_1 = 0°, \theta_2 = 180°$, and $\theta_3 = 0°$ (red IFEDF curve in Figure 3(b)) is investigated below as an example case.

First, the temporal evolution of the grounded electrode sheath width and voltage is shown in Figure 6(a). At this combination of phase angles, the grounded electrode sheath voltage is high for a long fraction of the RF period and collapses for a short fraction only. The sheath voltage exhibits multiple maxima and minima within one period of the fundamental driving frequency due to the harmonic modulation of the applied voltage. The oscillations, that are well observable in the sheath voltage around its maximum

Plasma Process Polym **2017,** *14*, 1600117

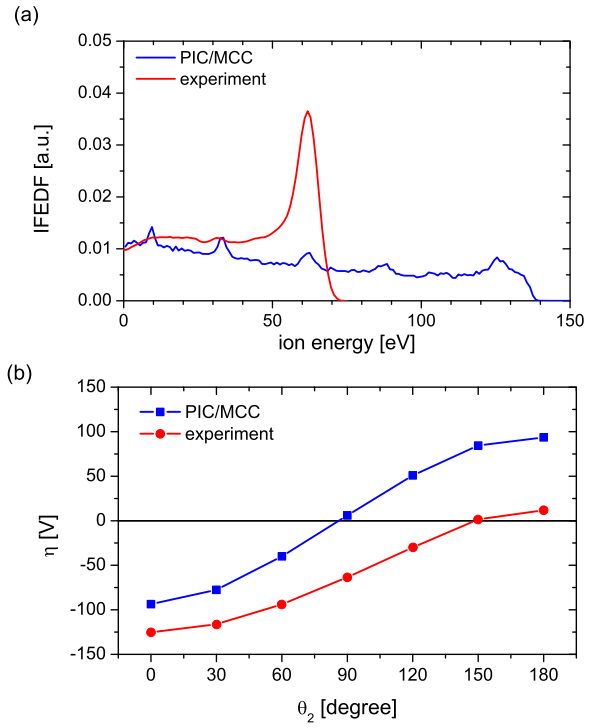

Figure 5. (a) Comparison of the IFEDFs for $\theta_2 = 180^\circ$ and (b) DC self-bias, η, for various phase angles of the second harmonic component, obtained from PIC/MCC simulations and experiments of a capacitive triple-frequency discharge in argon at 5 Pa. The applied voltage is 120 V at 13.56 MHz + 80 V at 27.12 MHz + 40 V at 40.68 MHz. The phases θ_1 and θ_3 are set to 0°.

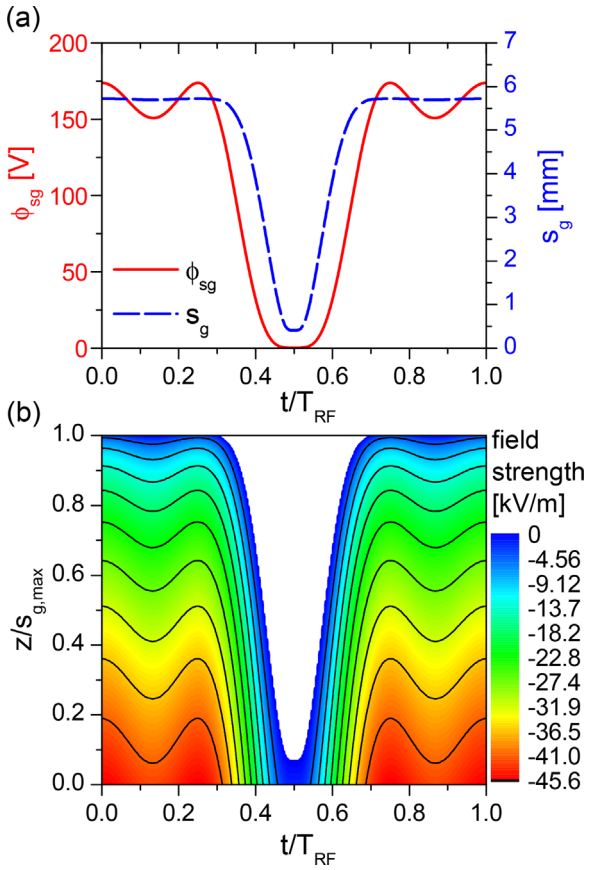

Figure 6. (a) Grounded electrode sheath voltage (red solid line, left axis) and width (blue dashed line, right axis) as a function of time obtained from the model. (b) Spatio-temporal distribution of the electric field in the grounded electrode sheath region obtained from the model. (Argon, 5 Pa, 120 V at 13.56 MHz + 80 V at 27.12 MHz + 40 V at 40.68 MHz, phases $\theta_1 = 0^\circ$, $\theta_2 = 180^\circ$, and $\theta_3 = 0^\circ$).

value (at $0.0 \leq t/T_{RF} \leq 0.3$ and $0.7 \leq t/T_{RF} \leq 1.0$) are hardly visible in the sheath width due to the "frequency coupling effect"[9]: if the sheath voltage changes but the sheath width is large, the local ion density is relatively large so that the modulation in the sheath width is weak. Moreover, although the floating potential is low (below 1 V), it leads to a residual sheath width at the time of minimum sheath voltage.

The spatio-temporal distribution of the electric field, depicted in Figure 6(b), is high for a long fraction of the fundamental RF period. It is small only for a short time around $t/T \approx 0.5$, when the grounded electrode sheath is collapsed. At each time, the field strength decreases with increasing distance from the electrode and vanishes completely at the momentary plasma sheath edge. Again, it is apparent that the temporal modulation is affected by the triple-frequency applied voltage waveform.

The temporally averaged, spatially resolved IEDF (see Figure 7(a)) shows the number of ions found within a certain energy interval at each position in the sheath. As the ions enter the sheath with a small energy and are accelerated by the RF electric field, the IFEDF spreads toward higher energies from $z = s_{max,g}$ to $z = 0$. Charge-exchange collisions lead to a "band" of ions between zero energy and the energy of the primary ions (originating from the bulk) at each position. The number of ions in this band is modulated: There is a fixed number of peaks that spread almost evenly over the energy interval of the "band."

As shown in Figure 7(b), the total ion flux at the grounded electrode (shown in Figure 3(b), as well) can be split into that of primary ions and that of secondary ions. The flux of primary ions (originating from the flow of ions out of the bulk into the sheath region) leads to a relatively narrow distribution around the maximum ion energy. The ion transit time is the most important quantity for the width of this structure. Due to the relatively long transit time (compared with the RF period), all primary ions "feel" almost the same acceleration in the electric field. The secondary ions, which are created in charge-exchange collision processes, arrive at the electrode with energies between zero and the energy of the primary ions. Peaks of high ion flux are found, that will be analyzed further below.

Figure 8(a) shows the energy an ion has upon its arrival at the grounded electrode depending on its starting position in

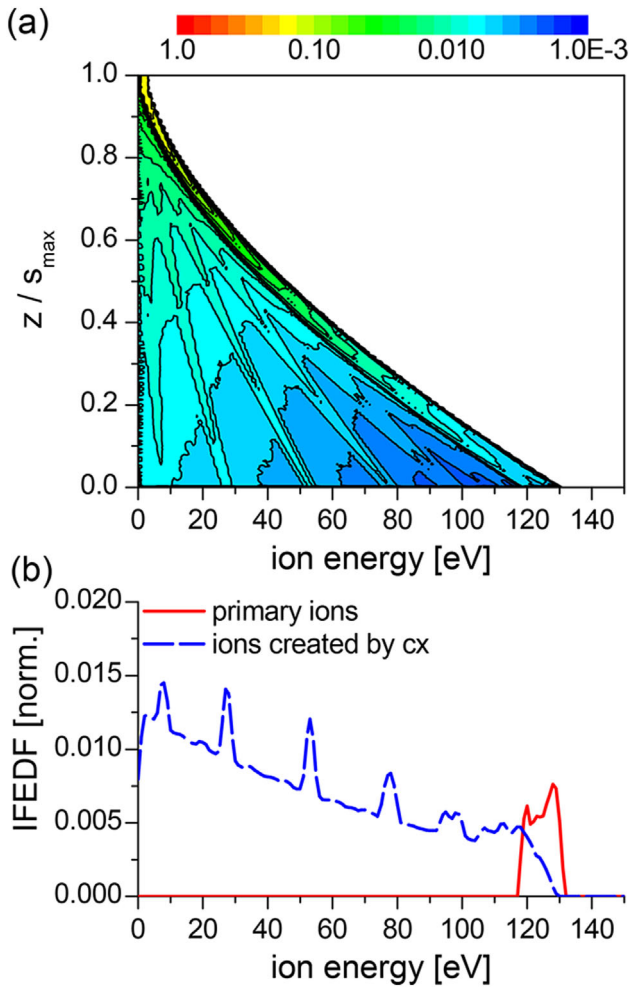

Figure 7. (a) Temporally averaged, spatially resolved ion energy distribution in the grounded electrode sheath region obtained from the model. The color scale provides the relative flux of ions on a total flux-normalized scale.(b) Contributions of primary ions and ions "born" in charge exchange collisions within the grounded electrode sheath region to the IFEDF at the grounded electrode obtained from the model. (Argon, 5 Pa, 120 V at 13.56 MHz + 80 V at 27.12 MHz + 40 V at 40.68 MHz, phases $\theta_1 = 0^\circ$, $\theta_2 = 180^\circ$, and $\theta_3 = 0^\circ$).

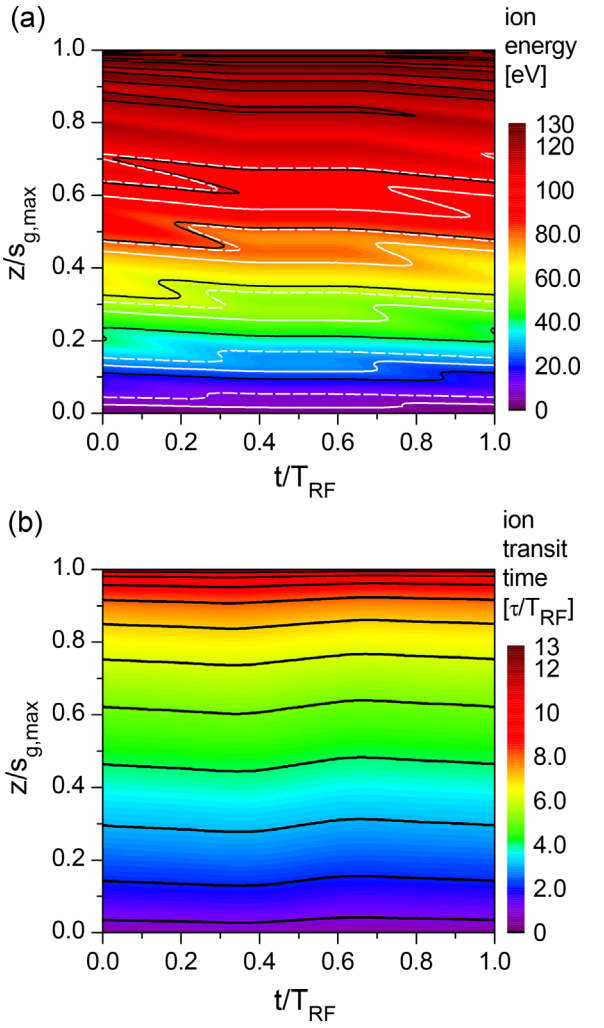

Figure 8. (a) Arrival energy of ions created by charge exchange collisions at different points in space time within the grounded electrode sheath region obtained from the model. The white solid and dashed lines indicate the minimum and maximum of the energy intervals of the peaks in the IEDF. (b) Transit time (normalized by T_{RF}) of ions created by charge exchange collisions at different points in space time within the grounded electrode sheath region obtained from the model. (Argon, 5 Pa, 120 V at 13.56 MHz + 80 V at 27.12 MHz + 40 V at 40.68 MHz, phases $\theta_1 = 0^\circ$, $\theta_2 = 180^\circ$, and $\theta_3 = 0^\circ$).

time and space within the grounded electrode sheath region (assuming that it does not collide). In general, the closer the starting position of the ions is to the electrode, the smaller the ion arrival energy. This is because these ions move a shorter distance and are accelerated for a shorter time until they arrive at the electrode. Furthermore, the temporal variation of the ion arrival energy is weak. Due to the RF modulation of the electric field, however, the ion energy can first decrease slightly and then increase again as a function of the spatial position ("zig-zag"-shaped parts of the black lines). This is because the acceleration becomes much stronger with decreasing distance from the electrode due to the much stronger electric field (shown above). On the one hand, an ion originating at a certain position in space time may impinge on the electrode just before the sheath collapse, that is, around $t/T_{RF} \approx 0.3$, so that the energy gain over the last fraction of the ion trajectory is very high. On the other hand, an ion originating at a position slightly further away from the electrode may impinge on the electrode after the sheath collapse, that is, around $t/T_{RF} \approx 0.7$, so that the energy gain over the last fraction of the ion trajectory is comparatively small. Thus, the ion energy can be slightly higher for slightly lower $z/s_{max,g}$ values, depending on the arrival time and the

corresponding acceleration in the last RF period of the total transit time.

Ions, that are created at $t/T_{rf} \approx 0.3$ and $z/s_{max,g} \approx 0.5$, for instance, gain only very little energy before the sheath collapses around $t/T_{rf} \approx 0.5$. Therefore, they arrive at the electrode with almost the same energy as those ions, that are created until $t/T_{rf} \approx 0.7$ at about the same position $z/s_{max,g} \approx 0.5$. All of these ions, in turn, gain only a little kinetic energy during their first RF period. Therefore, all ions that start within a spatio-temporal window – indicated by the white solid and dashed lines, that correspond to the minimum and maximum of the energy intervals of the peaks in the IEDF – will arrive with about the same energy.

The transit time of ions (τ, normalized by T_{RF}), that is, the time between their creation in a charge-exchange collision process and their arrival at the grounded electrode, becomes longer with increasing distance from the electrode (see Figure 8(b)). A more detailed analysis reveals that the lines corresponding to integer values of the normalized transit time are located within the regions of the starting positions in space and time of those ions, that contribute to the peaks in the IFEDF (compare Figure 8(a)). Accordingly, ions that start at a slightly later time but have a slightly shorter transit time, arrive at the same time within the RF period at the electrode and, due to a similar energy gain over the last RF periods of the total transit time, impinge on the electrode with about the same ion energy. This leads to the formation of the peaks in the IFEDF.

Moreover, the total flux of ions in the IFEDF at the grounded electrode can be split into different flux fractions of ions with different transit times from their starting position

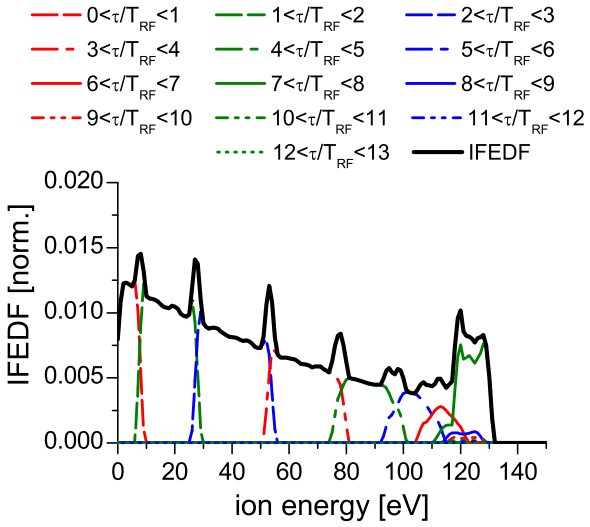

Figure 9. Contribution of ions with different normalized transit times from their starting location to the grounded electrode obtained from the model. (Argon, 5 Pa, 120 V at 13.56 MHz + 80 V at 27.12 MHz + 40 V at 40.68 MHz, phases $\theta_1 = 0^\circ$, $\theta_2 = 180^\circ$, and $\theta_3 = 0^\circ$).

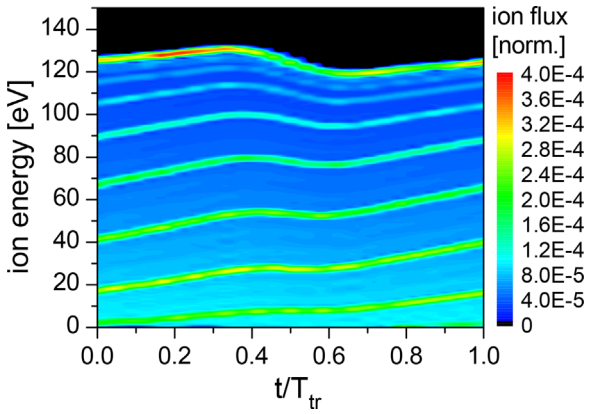

Figure 10. Distribution of ions arriving at the grounded electrode as a function of energy and time within the RF period obtained from the model. (Argon, 5 Pa, 120 V at 13.56 MHz + 80 V at 27.12 MHz + 40 V at 40.68 MHz, phases $\theta_1 = 0^\circ$, $\theta_2 = 180^\circ$, and $\theta_3 = 0^\circ$. The color scale provides the relative flux of ions on a total flux-normalized scale.

to the grounded electrode (see Figure 9). This is another way of visualizing the effect, that the peaks in the IFEDF are caused by ions with a transit time, that is close to an integer number of RF periods. In other words, ions with a transit time of just below three T_{rf}, for instance, may arrive with a slightly higher energy than those ions with a transit time of just above three T_{rf}, due to the reasons mentioned above. Hence, a peak is found in this overlapping energy region.

Finally, the model allows for a distinction of the energy distribution functions of ions at the grounded electrode at different times within the RF period. This is shown in Figure 10. The ion flux exhibits the peak structure mentioned above. Here, however, it becomes visible that the energy of these peaks changes as a function of time. This is because of the ions that arrive at different times experience different energy gains (most importantly during the last RF period of the transit time of the respective ions) in the RF electric field. The sheath is collapsed around $t/T_{rf} \approx 0.5$. Therefore, ions that arrive shortly after the collapse experience a very weak field during the last fraction of the transit time. As a consequence, the energy of all features in the IFEDF is reduced around $t/T_{rf} \approx 0.5$. After that (between $t/T_{rf} \approx 0.6$ and $t/T_{rf} \approx 0.4$ (or 1.4)), the energy of the features in the IFEDF increases as the acceleration of the ions becomes stronger due to the longer time spent in the region of high electric field close to the electrode. This modulation leads to the observation of peaks superimposed on a broad "band" in the IFEDF.

4. Conclusion

A simple model for the IFEDF in single- and multi-frequency CCRF plasmas was developed. By comparing the IFEDFs

from this model with the results of PIC/MCC simulations and RFEA measurements, it was shown that the model works in both symmetric and asymmetric discharge configurations.

In particular, it was demonstrated that the model is capable of reproducing the IFEDFs obtained from PIC/MCC simulations at various driving frequencies and pressures. For an electrically asymmetric scenario of a plasma driven by three consecutive harmonics, the phase angle of the second harmonic is a control parameter for the DC self-bias and, therefore, for the mean sheath voltages and the ion energies at the electrodes. Accordingly, the IFEDF changes. The results of the model were compared to simulations and experimental data of triple-frequency CCRF plasmas with very good agreement.

Further, the model was then used to investigate the ion dynamics in the multi-frequency RF sheath in detail. The temporal evolution of the sheath width and voltage were discussed. Based on the spatially and temporally resolved electric field, the IFEDF as a function of position, the role of primary ions and ions created in charge-exchange collision processes, the transit time and arrival energy of the ions as a function of their starting position in the sheath region, the contribution of ions with different transit times to the IFEDF at the electrode, and the time resolved IFEDF at the electrode were determined and discussed. The physical mechanisms behind the formation of peaks in the IFEDF were highlighted.

The model can be adapted to a large variety of discharge conditions and can be a useful tool to predict the IFEDF in CCRF plasmas. This is very important for surface processing applications, where the impact energy of the ions is of crucial importance. In the future, the detailed knowledge of the ion dynamics and the possibilities of tailoring the IFEDF shape should be combined with other methods, such as thermal probes[64] and plasma monitoring, to determine the role of the energy influx by ions in applications.

Acknowledgments: We thank James Franek, Steven Brandt, and Birk Berger (West Virginia University) for helpful discussions. This work was supported by the grant NKFIH 119357. The authors gratefully acknowledge support by the DFG (German Research Foundation) within the framework of the Sonderforschungsbereich SFBTR 87 and by the US National Science Foundation (grant PHY 1601080).

Received: June 30, 2016; Revised: October 7, 2016; Accepted: October 11, 2016; DOI: 10.1002/ppap.201600117

Keywords: capacitively coupled radio frequency plasmas; ion bombardment; ion-energy distribution function (IEDF); plasma modeling; radio frequency glow discharges (RFGD)

[1] M. A. Lieberman, A. J. Lichtenberg, "*Principles of Plasma Discharges and Materials Processing*," 2nd edition, Wiley, New York **2005**.
[2] P. Chabert, N. Braithwaite, "*Physics of Radio Frequency Plasmas*," Cambridge University Press, New York **2011**.
[3] Ch. Hollenstein, A. A. Howling, Ph. Guittienne, I. Furno, *Plasma Phys. Contr. Fusion* **2015**, *7*, 014010.
[4] Z. Donkó, J. Schulze, U. Czarnetzki, A. Derzsi, P. Hartmann, I. Korolov, E. Schüngel, *Plasma Phys. Cont. Fusion* **2012**, *54*, 124003.
[5] T. Kitajima, Y. Takeo, Z. Lj. Petrović, T. Makabe, *Appl. Phys. Lett.* **2000**, *77*, 489.
[6] V. Georgieva, A. Bogaerts, *Plasma Sources Sci. Technol.* **2006**, *15*, 368.
[7] P. C. Boyle, A. R. Ellingboe, M. M. Turner, *Plasma Sources Sci. Technol.* **2004**, *13*, 493.
[8] D. Gahan, B. Dolinaj, M. B. Hopkins, *Rev. Sci. Instrum.* **2008**, *79*, 033502.
[9] T. Gans, J. Schulze, D. O'Connell, U. Czarnetzki, R. Faulkner, A. R. Ellingboe, M. M. Turner, *Appl. Phys. Lett.* **2006**, *89*, 261502.
[10] Q. -Z. Zhang, Y. -N. Wang, A. Bogaerts, *J. Appl. Phys.* **2014**, *115*, 223302.
[11] B. G. Heil, U. Czarnetzki, R. P. Brinkmann, T. Mussenbrock, *J. Phys. D* **2008**, *41*, 165202.
[12] J. Schulze, E. Schüngel, U. Czarnetzki, *J. Phys. D* **2009**, *42*, 092005.
[13] U. Czarnetzki, J. Schulze, E. Schüngel, Z. Donkó, *Plasma Sources Sci. Technol.* **2011**, *20*, 024010.
[14] S. Bienholz, T. Styrnoll, P. Awakowicz, *J. Phys. D* **2014**, *47*, 065201.
[15] E. Schüngel, J. Schulze, Z. Donkó, U. Czarnetzki, *Phys. Plasmas* **2011**, *18*, 013503.
[16] J. Schulze, E. Schüngel, Z. Donkó, U. Czarnetzki, *J. Phys. D* **2010**, *43*, 225201.
[17] J. Schulze, E. Schüngel, Z. Donkó, U. Czarnetzki, *Plasma Sources Sci. Technol.* **2011**, *20*, 015017.
[18] T. Lafleur, P. A. Delattre, E. V. Johnson, J. P. Booth, *Appl. Phys. Lett.* **2012**, *101*, 124104.
[19] P. Diomede, D. J. Economou, T. Lafleur, J. P. Booth, S. Longo, *Plasma Sources Sci. Technol.* **2014**, *23*, 065049.
[20] E. Schüngel, S. Mohr, J. Schulze, U. Czarnetzki, M. J. Kushner, *Plasma Sources Sci. Technol.* **2014**, *23*, 015001.
[21] E. V. Johnson, P. A. Delattre, J. -P. Booth, *Appl. Phys. Lett.* **2012**, *100*, 133504.
[22] E. V. Johnson, S. Pouliquen, P. A. Delattre, J. -P. Booth, *J. Non-Cryst. Solids* **2012**, *358*, 1974.
[23] B. Bruneau, M. Lepecq, J. Wang, J. -C. Dornstetter, J. -L. Maurice, E. V. Johnson, *IEEE J. Photovolt.* **2014**, *4*, 1354.
[24] E. Schüngel, R. Hofmann, S. Mohr, J. Schulze, J. Röpcke, U. Czarnetzki, *Thin Solid Films* **2015**, *574*, 60.
[25] E. Schüngel, S. Mohr, J. Schulze, U. Czarnetzki, *Appl. Phys. Lett.* **2015**, *106*, 054108.
[26] B. Bruneau, T. Novikova, T. Lafleur, J. P. Booth, E. V. Johnson, *Plasma Sources Sci. Technol.* **2014**, *23*, 065010.
[27] B. Bruneau, T. Gans, D. O'Connell, A. Greb, E. V. Johnson, J. P. Booth, *Phys. Rev. Lett.* **2015**, *114*, 125002.
[28] B. Bruneau, T. Lafleur, T. Gans, D. O'Connell, A. Greb, I. Korolov, A. Derzsi, Z. Donkó, S. Brandt, E. Schüngel, J. Schulze, P. Diomede, D. J. Economou, S. Longo, E. Johnson, J. -P. Booth, *Plasma Sources Sci. Technol.* **2016**, *25*, 01LT02.
[29] J. Franek, S. Brandt, B. Berger, M. Liese, M. Barthel, E. Schüngel, J. Schulze, *Rev. Sci. Instrum.* **2015**, *86*, 053504.
[30] D. J. Coumou, T. Kummerer, D. Sullivan, *IEEE Trans. Plasma Sci.* **2014**, *42*, 1880.

[31] T. Mussenbrock, *Contrib. Plasma Phys.* **2012**, *52*, 571.
[32] E. Schüngel, Z. Donkó, P. Hartmann, A. Derzsi, I. Korolov, J. Schulze, *Plasma Sources Sci. Technol.* **2015**, *24*, 045013.
[33] B. Bruneau, T. Lafleur, J. -P. Booth, E. Johnson, *Plasma Sources Sci. Technol.* **025006**, *25*.
[34] E. Kawamura, V. Vahedi, M. A. Lieberman, C. K. Birdsall, *Plasma Sources Sci. Technol.* **1999**, *8*, R45.
[35] S. G. Ingram, N. St. J. Braithwaite, *J. Appl. Phys.* **1990**, *68*, 5519.
[36] C. Wild, P. Koidl, *J. Appl. Phys.* **1991**, *69*, 2909.
[37] M. Zeuner, H. Neumann, J. Meichsner, *J. Appl. Phys.* **1997**, *81*, 2985.
[38] D. Israel, K. -U. Riemann, L. Tsendin, *J. Appl. Phys.* **2006**, *99*, 093303.
[39] W. -C. Chen, Y. -K. Pu, *J. Phys. D* **2014**, *47*, 345201.
[40] U. Flender, K. Wiesemann, *J. Phys. D* **1994**, *27*, 509.
[41] D. Gahan, S. Daniels, C. Hayden, D. O'Sullivan, M. B. Hopkins, *Plasma Sources Sci. Technol.* **2012**, *21*, 015002.
[42] S. -B. Wang, A. E. Wendt, *J. Appl. Phys.* **2000**, *88*, 643.
[43] B. Jacobs, W. Gekelman, P. Pribyl, M. Barnes, *Phys. Rev. Lett.* **2010**, *105*, 075001.
[44] T. Baloniak, R. Reuter, C. Fĺ'otgen, A. von Keudell, *J. Phys. D* **2010**, *43*, 055203.
[45] A. Metze, D. W. Ernie, H. J. Oskam, *J. Appl. Phys.* **1989**, *65*, 993.
[46] T. E. Sheridan, J. Goree, *Phys. Fluids B* **1991**, *3*, 2796.
[47] M. A. Sobolewski, *Phys. Rev. E* **2000**, *62*, 8540.
[48] J. Robiche, P. C. Boyle, M. M. Turner, A. R. Ellingboe, *J. Phys. D* **2003**, *36*, 1810.
[49] U. Czarnetzki, *Phys. Rev. E* **2013**, *88*, 063101.
[50] M. M. Turner, P. Chabert, *Appl. Phys. Lett.* **2014**, *104*, 164102.
[51] B. Berger, S. Brandt, J. Franek, E. Schüngel, M. Koepke, T. Mussenbrock, J. Schulze, *J. Appl. Phys.* **2015**, *118*, 223302.
[52] E. Schüngel, S. Brandt, I. Korolov, A. Derzsi, Z. Donkó, J. Schulze, *Phys. Plasmas* **2015**, *22*, 043512.
[53] E. Schüngel, S. Brandt, Z. Donkó, I. Korolov, A. Derzsi, J. Schulze, *Plasma Sources Sci. Technol.* **2015**, *24*, 044009.
[54] J. Schulze, Z. Donkó, A. Derzsi, I. Korolov, E. Schüngel, *Plasma Sources Sci. Technol.* **2015**, *24*, 015019.
[55] M. Shihab, A. T. Elgendy, I. Korolov, A. Derzsi, J. Schulze, D. Eremin, T. Mussenbrock, Z. Donkó, R. P. Brinkmann, *Plasma Sources Sci. Technol.* **2013**, *22*, 055013.
[56] A. V. Phelps, **1994**, http://jilaww.colorado.edu/~avp/collision_data unpublished.
[57] A. V. Phelps, Z. Lj. Petrović, *Plasma Sources Sci. Technol.* **1999**, *8*, R21.
[58] A. V. Phelps, *J. Appl. Phys.* **1994**, *76*, 747.
[59] R. Kollath, "*Encyclopedia of Physics*," vol. 21 S. Flügge Ed., Springer, Berlin **1956**, p. 264.
[60] R. P. Brinkmann, *J. Appl. Phys.* **2007**, *102*, 093303.
[61] C. Böhm, J. Perrin, *Rev. Sci. Instrum.* **1993**, *64*, 31.
[62] J. K. Lee, O. V. Manuilenko, N. Yu. Babaeva, H. C. Kim, J. W. Shon, *Plasma Sources Sci. Technol.* **2005**, *14*, 89.
[63] U. Flender, K. Wiesemann, *J. Phys. D* **1994**, *27*, 509.
[64] M. Wolter, M. Stahl, H. Kersten, *Plasma Process. Polym.* **2009**, *6*, 626.